Q. J. R. Meteorol. Soc. (2000), **126**, pp. 2671–2689

Small-amplitude coastally trapped disturbances and the reduced-gravity shallow-water approximation

By DALE R. DURRAN*
University of Washington, USA

(Received 20 August 1999; revised 28 March 2000)

SUMMARY

Solutions are obtained for linear hydrostatic disturbances propagating parallel to the face of an uninterrupted topographic step in an infinitely deep, stably stratified fluid on an f-plane. These waves are vertically trapped because their frequencies are smaller than the Coriolis parameter and the height of the topographic step is finite. These waves are referred to as *step-trapped Kelvin waves*, because they are dynamically similar to internal Kelvin waves throughout the layer of fluid below the top of the topographic step. These waves appear to provide an idealized, semi-analytic model for the coastally trapped disturbances observed to propagate parallel to mountainous coastlines in several parts of the world.

Computations are performed for a basic state with uniform static stability and for a three-layer basic state in which the two lowest layers represent the marine boundary layer and a strong capping inversion. One might suppose that the linear dynamics of hydrostatic disturbances in the three-layer basic state could be well approximated by a reduced-gravity shallow-water model, but this is not the case. In particular, the reduced-gravity shallow-water model does not provide reliable estimates for the phase speed of linear step-trapped Kelvin waves. This defect suggests that detailed *quantitative* comparisons between marine boundary-layer flows and the reduced-gravity shallow-water system may not have any intrinsic physical significance. Nevertheless, these results do not preclude the possibility of constructing useful *qualitative* analogies between marine boundary-layer flows and the reduced-gravity shallow-water model.

KEYWORDS: Coastally trapped disturbances Kelvin waves Shallow-water equations

1. INTRODUCTION

Atmospheric disturbances have been observed to propagate along the flanks of extensive topographic barriers oriented parallel to coastlines in many parts of the world. One of the earliest dynamical theories for such disturbances was presented by Gill (1977), who proposed that the disturbances propagating around the southern end of Africa were essentially Kelvin waves, laterally trapped against the topography by Coriolis effects and vertically trapped by the strong marine inversion that is typically present along the southern African coast. Similar explanations were offered by Dorman (1985) for disturbances travelling along the west coast of North America and by Holland and Leslie (1986) for features propagating around the southern coast of Australia.

All of the preceding studies approximate the flow beneath an elevated inversion using a shallow-water model in which vertical displacements of the inversion layer are subject to a reduced gravitational restoring force g' equal to the true gravitational acceleration g times the fractional reduction in density across the inversion. The fractional decrease in density across the inversion is often evaluated in terms of the potential-temperature profile, in which case $g' = g\Delta\theta/\theta_0$, where $\Delta\theta$ is the increase in potential temperature across the inversion and θ_0 is the mean potential temperature within the inversion layer. The application of reduced-gravity shallow-water models to the study of atmospheric motions below an elevated inversion dates back at least to Freeman (1948), and has continued in many subsequent investigations of coastally trapped disturbances (CTDs) (e.g., Nguyen Ngoc Anh and Gill 1981; Bannon 1981; Reason and Steyn 1992; Rogerson and Samelson 1995; Samelson and Rogerson 1996). Reduced-gravity shallow-water models have also been used to investigate downslope windstorms (Long 1954) and low-level flow around bends in coastal topography (Winant *et al.* 1988).

* Corresponding address: University of Washington, Atmospheric Sciences, Box 351640, Seattle, WA 98195-1640, USA.

This paper examines the extent to which the reduced-gravity shallow-water model actually describes the dynamics of small-amplitude trapped waves propagating along a rigid side boundary in a continuously stratified fluid. Some aspects of this question were recently explored by Samelson (1999), who obtained expressions for the vertical structure of horizontally trapped modes in a stratified fluid on an f-plane bounded by a rigid sidewall of finite height. Samelson considered a problem in which a finite-depth layer of continuously stratified fluid was capped by an infinitely deep region of neutral stability. The neutral layer provides an artificial barrier to vertical energy propagation that is not present in real atmospheric profiles. In this paper the solution methodology presented by Samelson (1999) and Chapman (1982) is extended to problems with arbitrary variations in the basic-state stratification throughout an infinitely deep layer. Travelling vertically trapped waves are found to exist in an infinitely deep stratified fluid bounded by a rigid sidewall of finite height. The vertical trapping mechanism is discussed and is demonstrated to be independent of the presence of an elevated inversion. Even when the basic state contains a strong elevated inversion capping a weakly stratified marine boundary layer (MBL), the linear hydrostatic trapped waves actually supported by this basic state are found to be in poor agreement with the predictions of the reduced-gravity shallow-water model.

2. Vertical energy propagation in continuously stratified fluids

In order to develop a conceptual understanding of the processes by which CTDs are vertically trapped, we will briefly review the conditions under which internal waves propagate energy vertically in an incompressible rotating fluid. Let an overbar denote a horizontally uniform basic-state quantity; let ρ_0 be a constant reference density, and define

$$P = \frac{p - \overline{p}(z)}{\rho_0}, \quad b = -g\frac{\rho - \overline{\rho}(z)}{\rho_0}, \quad N^2 \equiv -\frac{g}{\rho_0}\frac{\partial \overline{\rho}}{\partial z},$$

where p is the pressure and ρ is the density. Then the Boussinesq equations, linearized about a basic-state at rest on an f-plane, may be written

$$u_t - fv + P_x = 0 \tag{1}$$

$$v_t + fu + P_y = 0 \tag{2}$$

$$w_t + P_z - b = 0 \tag{3}$$

$$b_t + N^2 w = 0 \tag{4}$$

$$u_x + v_y + w_z = 0, \tag{5}$$

or, equivalently, as

$$(w_{xx} + w_{yy} + w_{zz})_{tt} + f^2 w_{zz} + N^2(w_{xx} + w_{yy}) = 0 \tag{6}$$

(Gill 1982, p. 258), where the subscripts denote partial differentiation and u, v and w are the components of the wind in the x, y and z directions. Assuming that the domain is unbounded or periodic in the horizontal, wavelike solutions of the form $w = \widehat{w}(z)\, \mathrm{e}^{\mathrm{i}(kx+\ell y-\omega t)}$ exist provided that

$$\frac{\mathrm{d}^2\widehat{w}}{\mathrm{d}z^2} + \left(\frac{N^2 - \omega^2}{\omega^2 - f^2}\right)(k^2 + \ell^2)\widehat{w} = 0. \tag{7}$$

Suppose that N assumes a constant value of N_t above z_t and that $N_\mathrm{t} > f$. Then, if either $\omega > N_\mathrm{t}$ or $\omega < f$, solutions to (7) decay exponentially with height for all $z > z_\mathrm{t}$.

Now consider the behaviour of disturbances in the subdomain $x \leqslant 0$ when a rigid infinitely high vertical wall is located at $x = 0$. Classical internal Kelvin waves are solutions to this problem; their structure may be easily determined by by setting $u = 0$ in (1)–(5) to yield the reduced system

$$(w_{yy} + w_{zz})_{tt} + N^2 w_{yy} = 0 \tag{8}$$

$$w_{xzt} + f w_{yz} = 0.$$

This system is satisfied by modes of the form $w = \widehat{w}(z)\, \mathrm{e}^{f\ell x/\omega}\, \mathrm{e}^{\mathrm{i}(\ell y - \omega t)}$ provided that

$$\frac{\mathrm{d}^2\widehat{w}}{\mathrm{d}z^2} + \left(\frac{N^2 - \omega^2}{\omega^2}\right) \ell^2 \widehat{w} = 0. \tag{9}$$

Again assuming that $N = N_\mathrm{t}$ for $z > z_\mathrm{t}$, solutions to (9) will decay exponentially for $z > z_\mathrm{t}$ provided that $\omega > N_\mathrm{t}$. However, in contrast to the behaviour of internal gravity waves in a horizontally unbounded domain, there is no low-frequency threshold below which the vertical structure of the Kelvin wave transitions from sinusoidal oscillations to exponential decay with height. In particular, sub-inertial Kelvin waves (i.e. waves for which $\omega < f$) have a sinusoidal vertical structure.

These equations will be applied to the atmosphere, in which case the lower boundary condition on $\widehat{w}$ is that there be no flow normal to the rigid lower boundary of the fluid. The atmosphere has no distinct upper boundary, so the upper boundary condition is imposed in the limit $z \to \infty$. In order to assure the physical relevance of mathematical solutions to (7) in the infinitely deep atmosphere, those solutions must satisfy one of two possible conditions: either (i) the perturbation energy density must approach zero as $z \to \infty$, or (ii) if the perturbation energy density is finite as $z \to \infty$, then the perturbation energy flux associated with each individual vertically propagating mode must be upward. The second condition allows the representation of disturbances generated within the domain that propagate energy upward to arbitrarily great heights, but it prohibits downward propagating modes from radiating energy into the domain from infinity. Vertical standing waves that do not decay as $z \to \infty$ are prohibited by the second condition because standing waves have zero energy flux. Such waves are not physically realizable solutions *in an infinitely deep domain* because vertical standing waves are the sum of equal-amplitude modes propagating upward from within the domain and downward from infinity, and the downward radiating component of the standing wave is not physically realizable.

Now consider the circumstances under which non-trivial trapped waves can exist above a flat lower boundary in the presence of an infinitely high vertical sidewall. The lower boundary condition is simply $\widehat{w}(0) = 0$. Kelvin-wave modes can be vertically trapped if there is a sufficient decrease in N with height. As a simple example, suppose that the atmosphere has a two-layer structure with Brunt–Väisälä frequencies N_U and N_L in the upper and lower layers respectively, and that the depth of the lower layer is d. Trapped Kelvin waves having a sinusoidal vertical structure in the lower layer and exponential decay aloft exist in the two-layer system provided that ω and ℓ satisfy the dispersion relation

$$\cot\left[\ell d \left(\frac{N_\mathrm{L}^2}{\omega^2} - 1\right)^{1/2}\right] = -\left[\frac{\omega^2 - N_\mathrm{U}^2}{N_\mathrm{L}^2 - \omega^2}\right]^{1/2}, \tag{10}$$

which may be obtained by requiring the solutions to (8) and their vertical derivatives (and thereby the pressure) to match at the interface (Scorer 1949; Nance and Durran

1997). Real values of ω and ℓ satisfy (10) only when $N_U < \omega \leqslant N_L$. Internal Kelvin waves are not vertically trapped unless $N_U < \omega$. This criterion generalizes to multi-layer atmospheric structures with constant Brunt–Väisälä frequency and no mean flow in each layer, for which a necessary condition for vertical trapping is that the wave frequency must exceed the Brunt–Väisälä frequency in the topmost layer.

A representative value for the upper-tropospheric stability during CTD events off the west coast of the United States is 0.01 s^{-1}, which we will take as an estimate for N_U. Ignoring energy leakage into the stratosphere (which would require an even larger lower bound on ω), the frequencies of vertically trapped linear Kelvin waves must, therefore, exceed 0.01 s^{-1}. CTDs observed off the west coast of the United States typically propagate at a mean phase speed c_p of roughly 7–8 m s^{-1} (Bond *et al.* 1996). Thus, if these CTDs behave like linear vertically trapped internal Kelvin waves propagating along an infinitely high vertical sidewall, they must satisfy $\omega = c_p\ell > 0.01$ or, equivalently, their north–south horizontal wavelength λ must be less than approximately 5 km. There is no completely obvious choice for the north–south horizontal wavelength characteristic of actual west-coast CTDs, because CTDs usually do not contain periodically alternating regions of southerly and northerly flow. Bond *et al.* (1996) report that the average duration of the southerly flow at a given point is 30 hours, from which a rough estimate of the half-wavelength of the disturbance can be computed as the northward phase speed × 30 hours. Once again using the 7–8 m s^{-1} estimate of the phase speed by Bond *et al.* (1996), the total north–south wavelength of observed CTD is approximately 1600 km. Even allowing for the considerable uncertainty in the precise value of λ, it is obvious that the wavelength of observed CTDs is far in excess of the 5 km threshold above which internal Kelvin waves cease to be vertically trapped by the decrease in Brunt–Väisälä frequency above the marine inversion.

Using the preceding values for the typical phase speed and wavelength of west-coast CTDs, the typical frequency of these disturbances may be estimated as $\omega_{ctd} = 0.3 \times 10^{-4}$ s^{-1}. Although this estimate for ω_{ctd} does not come close to satisfying the vertical trapping criterion $\omega_{ctd} > N_L$, it does satisfy the vertical trapping criterion $\omega_{ctd} < f$ for internal gravity waves in a horizontally unbounded atmosphere. The coastally trapped disturbance presented in Fig. 1 of Gill (1977) is also sub-inertial; it has a period of approximately four days or, equivalently, a frequency of approximately 0.2×10^{-4} s^{-1}.

The crucial factors that appear to vertically trap small-amplitude CTDs are simply that (i) they are sub-inertial and (ii) they propagate along a topographic barrier of finite height. The vertical trapping of sub-inertial disturbances propagating around seamounts was demonstrated in numerical calculations by Brink (1989), but the importance of this trapping mechanism does not seem to have been identified in atmospheric problems. As will be detailed in the following section, small-amplitude vertically trapped waves may exist, propagating along the face of a vertical step of finite height in the topography underlying an infinitely deep, continuously stratified fluid. At elevations below the top of the step, small-amplitude disturbances with sub-inertial frequencies and oscillatory vertical structures similar to internal Kelvin waves are supported by the rigid sidewall. At elevations above the top of the step these disturbances are governed by (6), and since they are sub-inertial, they must decay as $z \to \infty$.

A conceptual model comparing the mechanisms that vertically trap internal Kelvin waves against an infinitely high sidewall, and against a sidewall of finite height, is shown in Fig. 1. In the case of an infinitely high sidewall, the vertical velocity varies sinusoidally throughout the depth of the lower layer and decays exponentially aloft. Only high-frequency modes for which $\omega > N_U$ are trapped; non-hydrostatic effects play

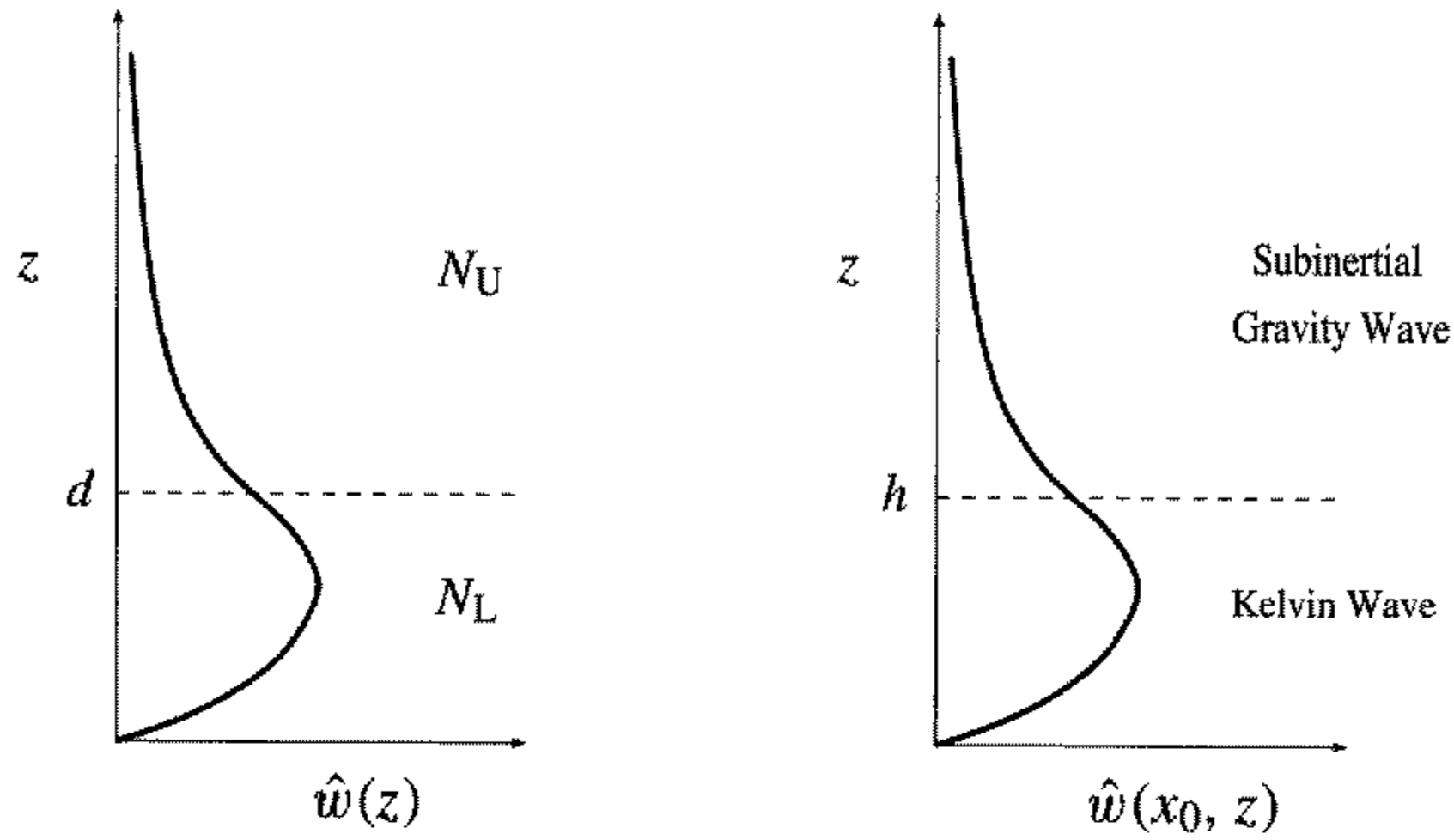

Figure 1. Schematic illustration of the vertical structure function $\hat{w}$ as a function of z. Left: non-hydrostatic Kelvin waves propagating along a infinitely high vertical sidewall trapped by the decrease in Brunt–Väisälä frequency with height in a two-layer atmosphere of depth d. Right: hydrostatic vertically trapped sub-inertial waves propagating along a vertical sidewall of height h in an atmosphere with uniform Brunt–Väisälä frequency.

a crucial role in trapping these waves. Now consider the case where the sidewall has finite height; then low-frequency modes with $\omega < f$ will be vertically trapped in the region above the step, but these modes, which will be referred to as *step-trapped Kelvin waves*, can have a non-trivial vertical structure similar to that of a conventional internal Kelvin wave in the region below the height of the topographic barrier. In contrast to the high-frequency Kelvin waves represented by the left profile in Fig. 1, the pressure perturbations in step-trapped Kelvin waves are essentially hydrostatic. A more detailed analysis of the step-trapped Kelvin wave is presented in the next two sections. As will become evident, the vertical and cross-barrier structures of these waves are non-separable, so the profile shown on the right in Fig. 1 actually represents the vertical structure of $\hat{w}$ at a specific location x_0.

3. Solution procedure

The procedure for evaluating the structure and speed of linear step-trapped Kelvin waves is an extension of that presented in an oceanic context by Chapman (1982) and applied to the atmosphere by Samelson (1999). These extensions permit the computation of step-trapped Kelvin waves when the Brunt–Väisälä frequency has an arbitrary vertical structure below the height of the step topography.

After invoking the hydrostatic approximation, (1)–(5) may be reduced to the single equation

$$\frac{\partial}{\partial t}\left[\frac{\partial^2 P}{\partial x^2}+\frac{\partial^2 P}{\partial y^2}+\left(\frac{\partial^2}{\partial t^2}+f^2\right)\frac{\partial}{\partial z}\left(\frac{1}{N^2}\frac{\partial P}{\partial z}\right)\right]=0. \tag{11}$$

Let x be the horizontal coordinate perpendicular to the face of the step topography, then waves propagating parallel to the face of the topographic step may be expressed in the

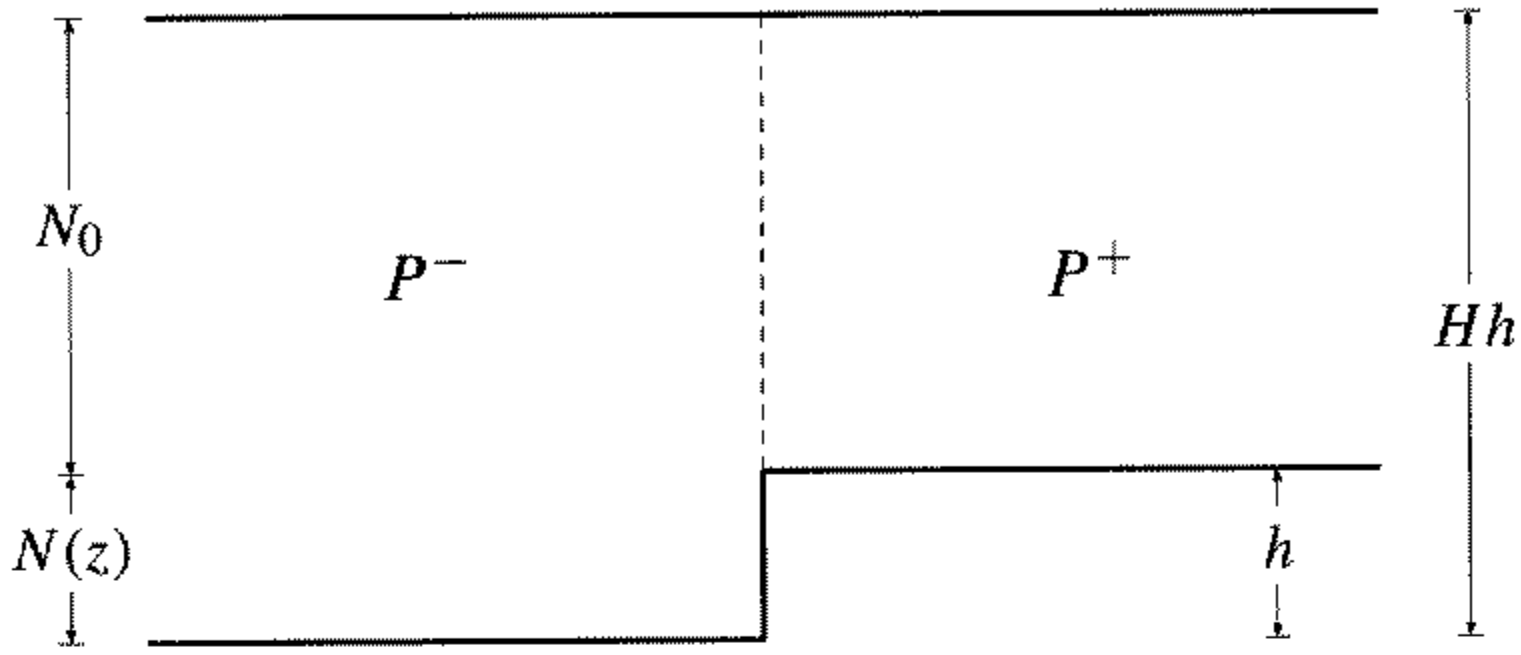

Figure 2. Cross-section of the domain normal to the face of the topographic step throughout which $\widehat{P}(x, z)$ is computed. The vertical distribution of the Brunt–Väisälä frequency is schematically indicated on the left.

functional form $P = \widehat{P}(x, z)\, e^{i(\ell y - \omega t)}$ which, upon substitution into (11), yields

$$\widehat{P}_{xx} + (f^2 - \omega^2)\left(\frac{\widehat{P}_z}{N^2}\right)_z - \ell^2 \widehat{P} = 0. \tag{12}$$

Solutions for $\widehat{P}$ are sought in the domain shown in Fig. 2, in which a horizontal lower boundary abruptly rises in a vertical wall of height h at $x = 0$ and then remains horizontal for $x > 0$. An upper boundary is imposed for computational purposes at $z = Hh$. The Brunt–Väisälä frequency is arbitrary for $0 < z < h$ and is a uniform value of N_0 for $z > h$.*

Let P^- and P^+ be defined as those subsets of the solution $\widehat{P}$ in the subdomains $x < 0$ and $x > 0$, respectively. P^- and P^+ are required to satisfy (12) and the following boundary conditions

$$P^- \to 0 \quad \text{as} \quad x \to -\infty, \qquad P^+ \to 0 \quad \text{as} \quad x \to \infty, \tag{13}$$

$$P_z^- = 0 \quad \text{at} \quad z = 0, \qquad P_z^+ = 0 \quad \text{at} \quad z = h, \tag{14}$$

$$P^- = 0 \quad \text{at} \quad z = Hh, \qquad P^+ = 0 \quad \text{at} \quad z = Hh. \tag{15}$$

The condition (14) is obtained by requiring the normal velocity to vanish at the lower boundary; (15) is a proxy for $\widehat{P} \to 0$ as $z \to \infty$. The sensitivity of the solution to this upper boundary condition will be discussed at the end of this section.

The pressure and horizontal velocities must also match at the interface, which yields the conditions that at $x = 0$

$$P^+ = P^- \quad \text{for} \quad h < z < Hh \tag{16}$$

$$\frac{\omega}{f\ell} P_x^- - P^- = \begin{cases} \dfrac{\omega}{f\ell} P_x^+ - P^+ & \text{for } h < z < Hh \\ 0 & \text{for } 0 < z < h. \end{cases} \tag{17}$$

Define a non-dimensional frequency $\sigma = \omega/f$, a non-dimensional Brunt–Väisälä frequency $\tilde{N} = N/N_0$, the Rossby radius of deformation $L_r = N_0 h/f$, and the parameter

$$\lambda = \ell L_r (1 - \sigma^2)^{-1/2}. \tag{18}$$

* The solution procedure can be trivially generalized to account for arbitrary profiles of N throughout the depth of the domain, but this modestly complicates the evaluation of P^+ and is not necessary for the present study.

Transforming coordinates such that

$$\xi = \frac{x}{L_r}(1-\sigma^2)^{1/2}, \quad \zeta = \frac{z}{h},$$

the governing equation (12) becomes

$$\widehat{P}_{\xi\xi} + \left(\frac{\widehat{P}_\zeta}{\widetilde{N}^2}\right)_\zeta - \lambda^2 \widehat{P} = 0, \tag{19}$$

and the matching condition (17) is

$$\frac{\sigma}{\lambda} P_\xi^- - P^- = \begin{cases} \dfrac{\sigma}{\lambda} P_\xi^+ - P^+ & \text{for } 1 < \zeta < H \\ 0 & \text{for } 0 < \zeta < 1. \end{cases} \tag{20}$$

Solutions to (19) and the boundary conditions (13)–(15) exist in the form

$$P^- = \sum_{n=0}^{N} a_n \, \mathrm{e}^{\alpha_n \xi} \phi_n(\zeta), \quad P^+ = \sum_{n=0}^{N} b_n \, \mathrm{e}^{-\beta_n \xi} \cos[\nu_n(\zeta - 1)]. \tag{21}$$

Here

$$\nu_n = \frac{(n+1/2)\pi}{H-1}, \quad \beta_n = (\nu_n^2 + \lambda^2)^{1/2},$$

and α_n and ϕ_n are eigenvalues and eigenvectors for the Sturm–Liouville problem

$$\frac{\mathrm{d}}{\mathrm{d}\zeta}\left(\frac{1}{\widetilde{N}^2}\frac{\mathrm{d}\phi}{\mathrm{d}\zeta}\right) + (\alpha^2 - \lambda^2)\phi = 0, \tag{22}$$

subject to the boundary conditions $\mathrm{d}\phi/\mathrm{d}\zeta = 0$ at $\zeta = 0$ and $\phi = 0$ at $\zeta = H$. In order to simplify the subsequent analysis, each ϕ_n is normalized such that

$$\int_0^H \phi_n^2(\zeta)\, \mathrm{d}\zeta = 1. \tag{23}$$

In the previous studies by Chapman (1982) and Samelson (1999), $\widetilde{N}$ was constant and (22) was solved analytically. In the present case $\widetilde{N}$ will be allowed to vary in the vertical in a manner representative of the marine boundary layer and capping inversion off the west coast of North America; (22) is therefore solved numerically using the finite-difference approximation

$$\frac{1}{(\Delta\zeta)^2}\left[\left(\frac{e_{k+1}-e_k}{\widetilde{N}^2_{k+\frac{1}{2}}}\right) - \left(\frac{e_k - e_{k-1}}{\widetilde{N}^2_{k-\frac{1}{2}}}\right)\right] + (\alpha^2 - \lambda^2)e_k = 0,$$

in which e_k approximates $\phi(k\Delta\zeta)$, and $\widetilde{N}_{k+\frac{1}{2}}$ is the non-dimensional Brunt–Väisälä frequency at $\zeta = (k+\frac{1}{2})\Delta\zeta$. The zero gradient condition at $\zeta = 0$ is approximated using a second-order one-sided derivative such that

$$3e_0 - 4e_1 + e_2 = 0.$$

The expansion coefficients a_n and b_n in (21) are evaluated using the matching conditions at $\xi = 0$ as follows. According to the pressure matching condition (16),

$$\sum_{n=0}^{N} a_n \phi_n(\zeta) = \sum_{n=0}^{N} b_n \cos[\nu_n(\zeta - 1)]$$

for $\zeta \in [1, H]$. Multiplying the preceding by $\cos \nu_m(\zeta - 1)$, integrating with respect to ζ over the interval $[1, H]$, and using the orthogonality of the Fourier modes, yields

$$b_m = \frac{2}{H-1} \sum_{n=0}^{N} r_{m,n}\, a_n, \tag{24}$$

where

$$r_{m,n} = \int_1^H \cos \nu_m(\zeta - 1)\phi_n(\zeta)\, \mathrm{d}\zeta. \tag{25}$$

The velocity matching condition (20) requires that

$$\sum_{n=0}^{N} \left(\frac{\sigma}{\lambda}\alpha_n - 1\right) a_n \phi_n = \begin{cases} -\sum_{n=0}^{N} \left(\frac{\sigma}{\lambda}\beta_n + 1\right) b_n \cos \nu_n(\zeta - 1) & \text{for } 1 < \zeta < H, \\ 0 & \text{for } 0 < \zeta < 1. \end{cases}$$

Multiplying the preceding by ϕ_m, integrating with respect to ζ over the interval $[0, H]$, and using (23), (25), and the orthogonality of the eigenfunctions to the Sturm–Liouville problem (22), the preceding reduces to

$$\left(\frac{\sigma}{\lambda}\alpha_m - 1\right) a_m = -\sum_{n=0}^{N} \left(\frac{\sigma}{\lambda}\beta_n + 1\right) r_{n,m} b_n, \tag{26}$$

Let $\mathbf{A}$ and $\mathbf{B}$ be diagonal matrices in which the ith diagonal elements are α_i and β_i, respectively. Let $\mathbf{R}$ be the matrix with elements $r_{m,n}$, and $\mathbf{a}$ be the vector whose ith element is a_i. Then (24) and (26) may be expressed as the single linear system

$$\frac{\sigma}{\lambda}\left(\mathbf{A} + \frac{2}{H-1}\mathbf{R}^{\mathrm{T}}\mathbf{B}\mathbf{R}\right)\mathbf{a} = \left(\mathbf{I} - \frac{2}{H-1}\mathbf{R}^{\mathrm{T}}\mathbf{R}\right)\mathbf{a}. \tag{27}$$

If λ is specified, the preceding becomes a generalized eigenvalue problem for the eigenvalues σ and eigenvectors $\mathbf{a}$. The actual along-step wave number for each mode can be computed from (18) after determining σ from (27).

Now consider the sensitivity of the solution to the upper boundary condition (15). At least for the parameter values considered in this paper, the waves decay rapidly with height and, as a consequence, the solution near the surface is quite insensitive to the elevation at which $\widehat{P}$ is artificially set to zero. This is illustrated in Fig. 3, which shows vertical profiles of P^- computed above the point $x = -L_{\mathrm{T}}/2$ for domain depths corresponding to $H = 2$, 3, 4 and 5. The results shown are for the lowest-order mode in an atmosphere with constant stratification.

The solutions shown in this paper were computed using MATLAB to evaluate (27). In all cases $H = 4$ which, as suggested by Fig. 3, will allow an accurate approximation to the true solution in an unbounded domain throughout the layer $0 \leqslant z/h \leqslant 2.5h$. In

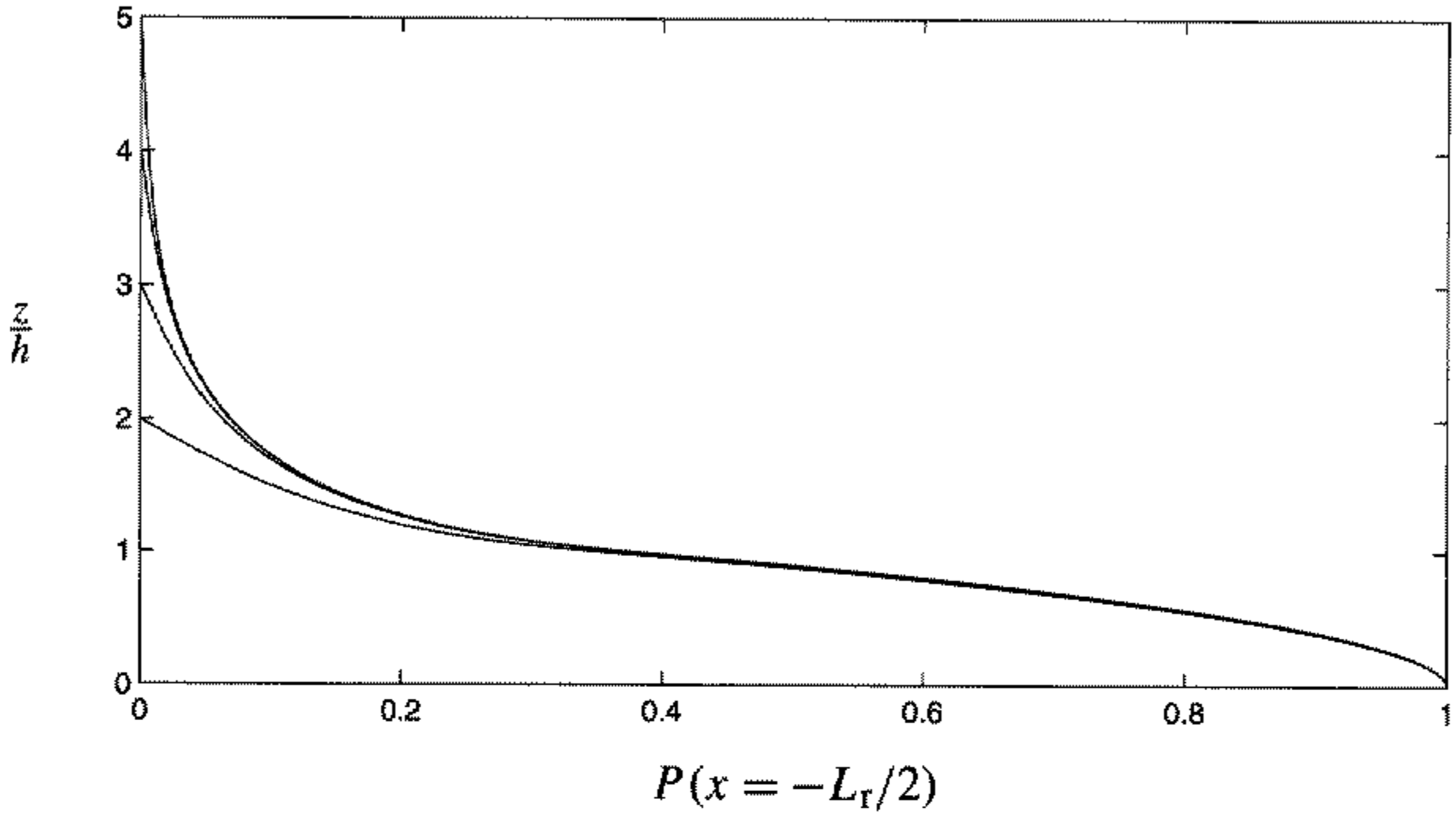

Figure 3. Vertical profiles of P^- for the lowest-order mode in a atmosphere with constant stability evaluated at $x = -L_r/2$. Individual curves correspond to solutions for which P^- is set to zero at $z/h = 2$, 3, 4 and 5.

those cases for which $h = 1$ km, 121 modes were retained in the expansions (21), and the eigenmodes for the Sturm–Liouville problem (22) were computed on a numerical mesh with 241 grid points. The integral (25) was evaluated at the same numerical resolution as ϕ_n using the trapezoidal rule. In those cases for which $h = 2$ km, 241 modes were retained in (21) and 481 grid points were used to compute the eigenmodes and their vertical integrals. As noted by Schmidt and Johnson (1993b), who considered a similar problem in an oceanic context, the pressure gradient is singular at the step and the solution is, therefore, difficult to evaluate accurately as $x \to 0$. Nevertheless, outside of the immediate neighbourhod of the step, $-0.03 < x/L_r < 0.03$, the solutions presented in this paper are not sensitive to further refinements in the preceding numerical parameters.

4. Step-trapped Kelvin waves

Figure 4 shows an x–z cross-section of pressure and velocity through a step-trapped Kelvin wave propagating along the face of a one-kilometre-high barrier in a basic state with a uniform Brunt–Väisälä frequency of 0.01 s^{-1}. Only the the bottom 60% of the domain, which extends to $z/h = 4$, is included in Fig. 4. No data are plotted in the region $-0.03 < x/L_r < 0.03$ because more than 121 expansion functions must be retained in (21) to determine the solution accurately very close to the face of the step. The wave shown in Fig. 4 is that eigenmode with no nodal lines below the top of the step (mode-0) satisfying (19) with $\lambda = 1$. The y-wavelength of this mode λ_y is 462 km and its phase speed is 5.0 m s^{-1}. This solution is similar to that shown in a different format in Fig. 5 of Samelson (1999), except that the computation shown here is performed in a much deeper domain and the horizontal and vertical axes are normalized in a manner that easily allows one to appreciate that the mode is vertically trapped. Below the top of the step the spatial structure of this mode is similar to that of a classical mode-0 linear Kelvin wave propagating at the same phase speed through a uniformly stratified fluid with Brunt–Väisälä frequency N_0 and a free surface at $z = h$. Above the topography, the wave amplitude decays rapidly with height. Note that the nodal line along which

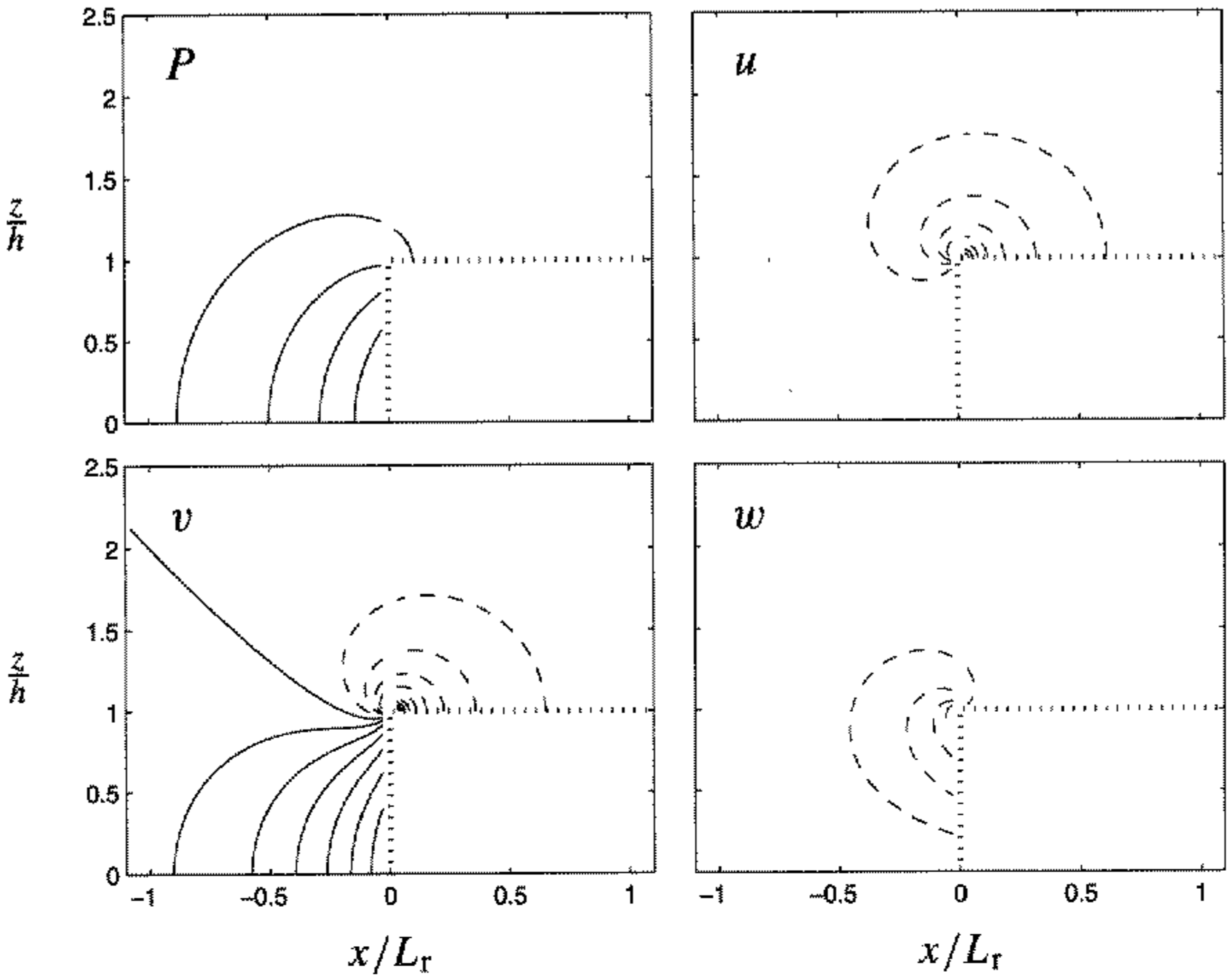

Figure 4. Cross-sections in the x–z plane through the mode-0 wave when N is constant. Individual panels show contours of P (at intervals of 0.2 $m^2 s^{-2}$), u and v (at intervals of 0.016 m s^{-1}), and w (at intervals of 2.0×10^{-4} m s^{-1}). Negative contours are dashed. The step topography is indicated by the dotted rectangle.

$v = 0$ is not parallel to either coordinate axis, implying that the spatial structure of the mode is non-separable, i.e. that v cannot be expressed as the product of functions of the form $s(x)$ and $r(z)$.

The horizontal structure of the pressure and horizontal velocity perturbations in the same mode-0 wave are shown in Fig. 5. Halfway up the face of the step, at $z/h = 0.5$, the polarization relations between the pressure and velocity fields are identical to those in a classical Kelvin wave—the horizontal velocity perturbations are parallel to the barrier and in phase with the pressure perturbations. Some cross-barrier flow is present further aloft, at $z/h = 1.3$, where the extrema in the pressure and velocity perturbations are roughly 2.5 times weaker than those at $z/h = 0.5$. The velocity field at $z/h = 0.5$ looks highly ageostrophic although, as in a classical Kelvin wave, the v component is actually close to geostrophic balance while the u component is approximately zero. At $z/h = 1.3$ the circulations around the extrema in the pressure field appear closer to geostrophic balance. A high degree of geostrophy should not be expected at $z/h = 1.3$, both because of the proximity of the terrain-induced ageostrophic forcing and because $\omega/f = 0.68$ for this mode, whereas ω/f is no larger than O(0.1) in the quasi-geostrophic limit.

The x–z structure of the mode-0 wave shown in Fig. 4 may be compared with that of the mode-1 wave shown in Fig. 6. As before, the solution shown in Fig. 6 is for the case $\lambda = 1$, $h = 1$ km, and a uniform Brunt–Väisälä frequency of 0.01 s^{-1}. The phase speed for this mode is 2.4 m s^{-1} and $\lambda_y = 609$ km. The mode-1 wave propagates more slowly and decays away from the topography more rapidly than the mode-0 wave shown in Fig. 4. The along-barrier horizontal velocity perturbations associated with a unit-amplitude pressure perturbation in the mode-1 wave are approximately 3.5 times greater than those associated with a unit-amplitude pressure perturbation in the mode-0 wave.

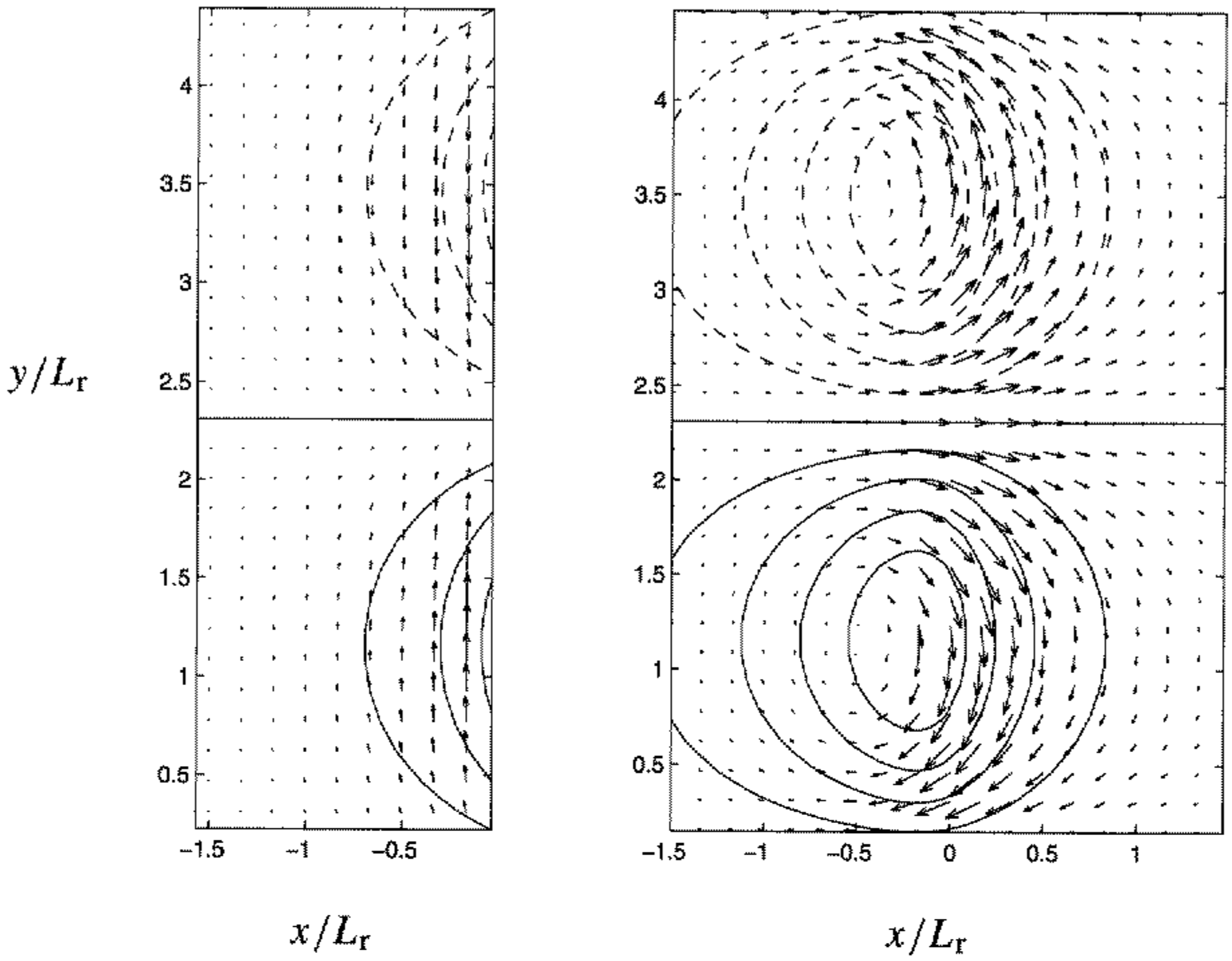

Figure 5. Horizontal cross-sections of perturbation pressure in the mode-0 wave shown in Fig. 4 at the heights $z/h = 0.5$ (contour interval is 0.25 m^2s^{-2}) and $z/h = 1.3$ (contour interval is 0.058 m^2s^{-2}). Also shown are the horizontal velocity vectors at each level. The vector magnitude is scaled differently at each level; the upper-level flow is significantly weaker.

Consistent with the reduction in ω/f for this mode to 0.25, the horizontal velocities above the topography (not show) are more nearly in geostrophic balance than those for the mode-0 wave.

Now consider how the preceding step-trapped Kelvin waves are modified when the atmospheric structure includes an idealized marine boundary layer (MBL) capped by a strong inversion. Ralph *et al.* (1998) present a detailed synthesis of observations taken as a CTD propagated along the central coast of California on 10–11 June 1994. Their data show that the MBL upstream of the CTD was approximately 250 m deep and was capped by an approximately 250 m thick inversion layer across which the temperature increased by 10–12 K. The true atmospheric structure off the California coast on 10–11 June 1994 will, therefore, be approximated by a three-layer profile in which the bottom two layers are each 250 mb thick and the static stabilities in the bottom, intermediate, and top layers are $N_L = 0.002$, $N_I = 0.035$, and $N_U = 0.01\ s^{-1}$, respectively. In order to avoid computing the vertical derivative of a discontinuous function in (19), the Brunt–Väisälä frequency is actually defined as

$$N(z) = \tfrac{1}{2}[N_L + N_U + (N_U - N_I)\tanh\{s(\zeta - \zeta_t)\} - (N_L - N_I)\tanh\{s(\zeta - \zeta_b)\}],$$

where $\zeta_b = 250/h$ and $\zeta_t = 500/h$ are the non-dimensional coordinates of the bottom and the top of the inversion layer, and $s = 100$. As before, h is specified as 1 km.

When the basic-state atmospheric profile includes the preceding idealized MBL and capping inversion, the x–z cross-sections of pressure and velocity through the

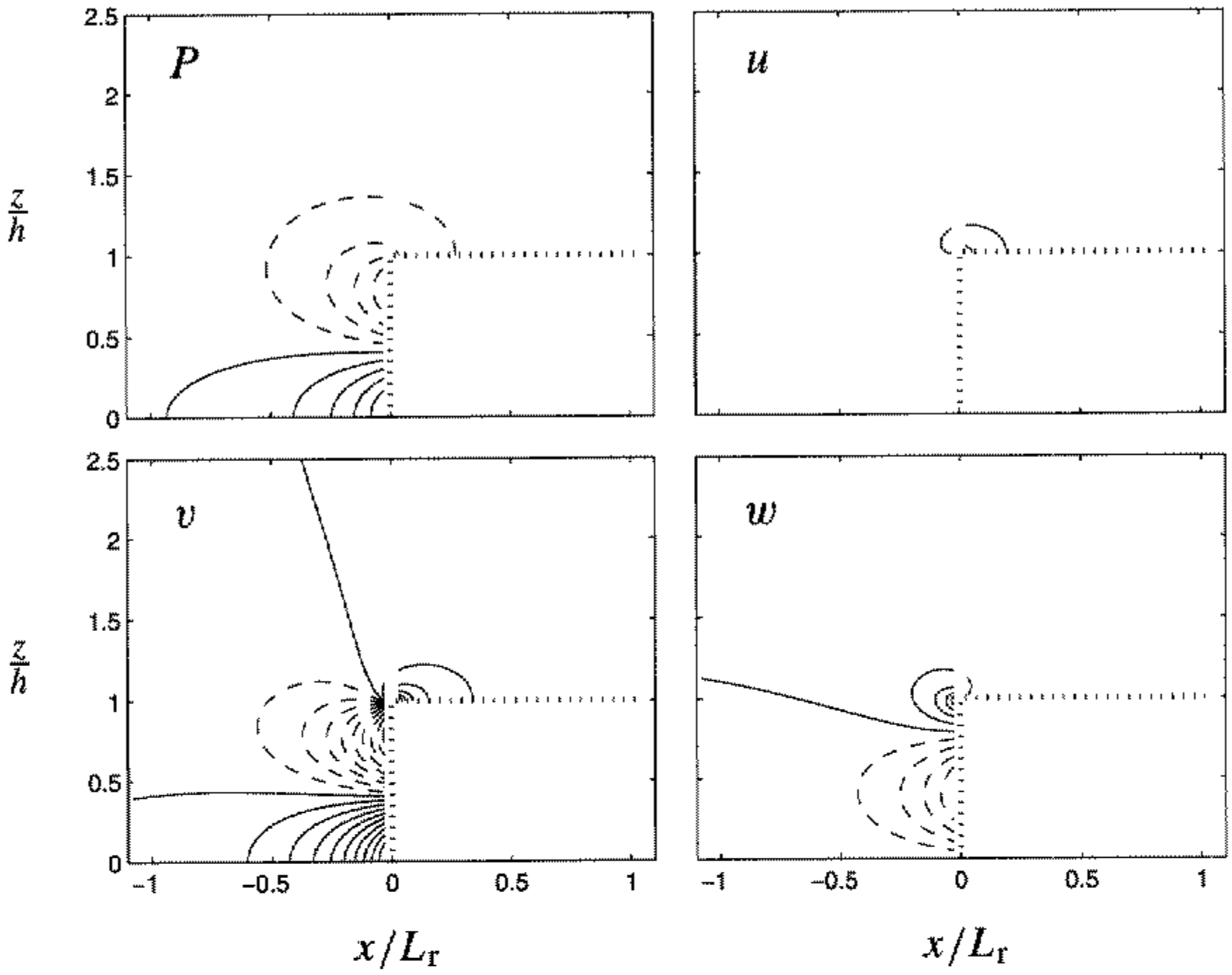

Figure 6. Cross-sections showing the x–z structure of the the mode-1 wave when N is constant. As in Fig. 4, except that the contour interval for u and v has been increased to 0.039 m s^{-1}.

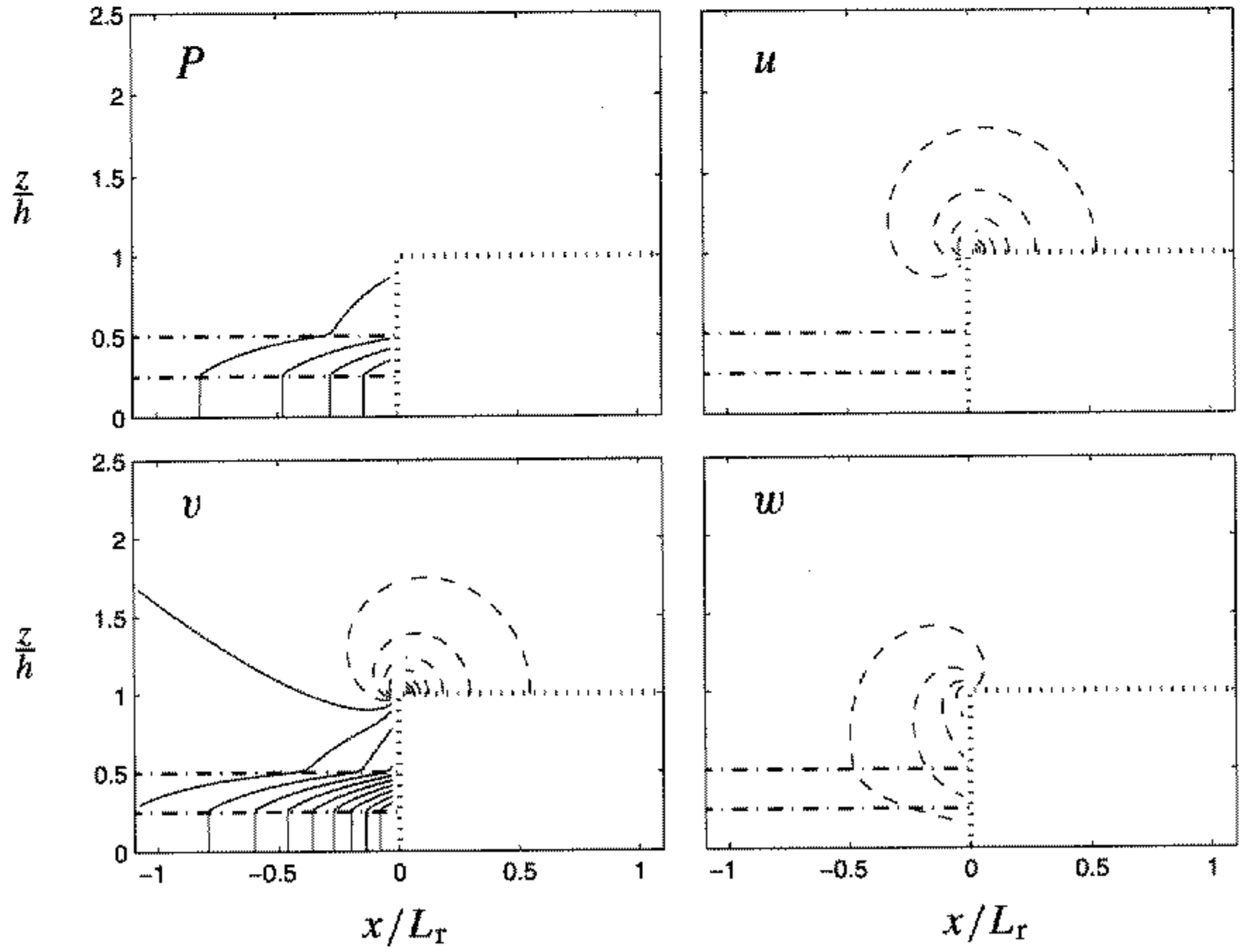

Figure 7. Cross-sections showing the x–z structure of the the mode-0 wave in the presence of an idealized MBL and capping inversion. As in Fig. 4, except that the contour interval for u and v is 0.0079 m s^{-1} and for w it is 7.8×10^{-5} m s^{-1}. Horizontal dash-dotted lines denote the top and bottom of the inversion layer.

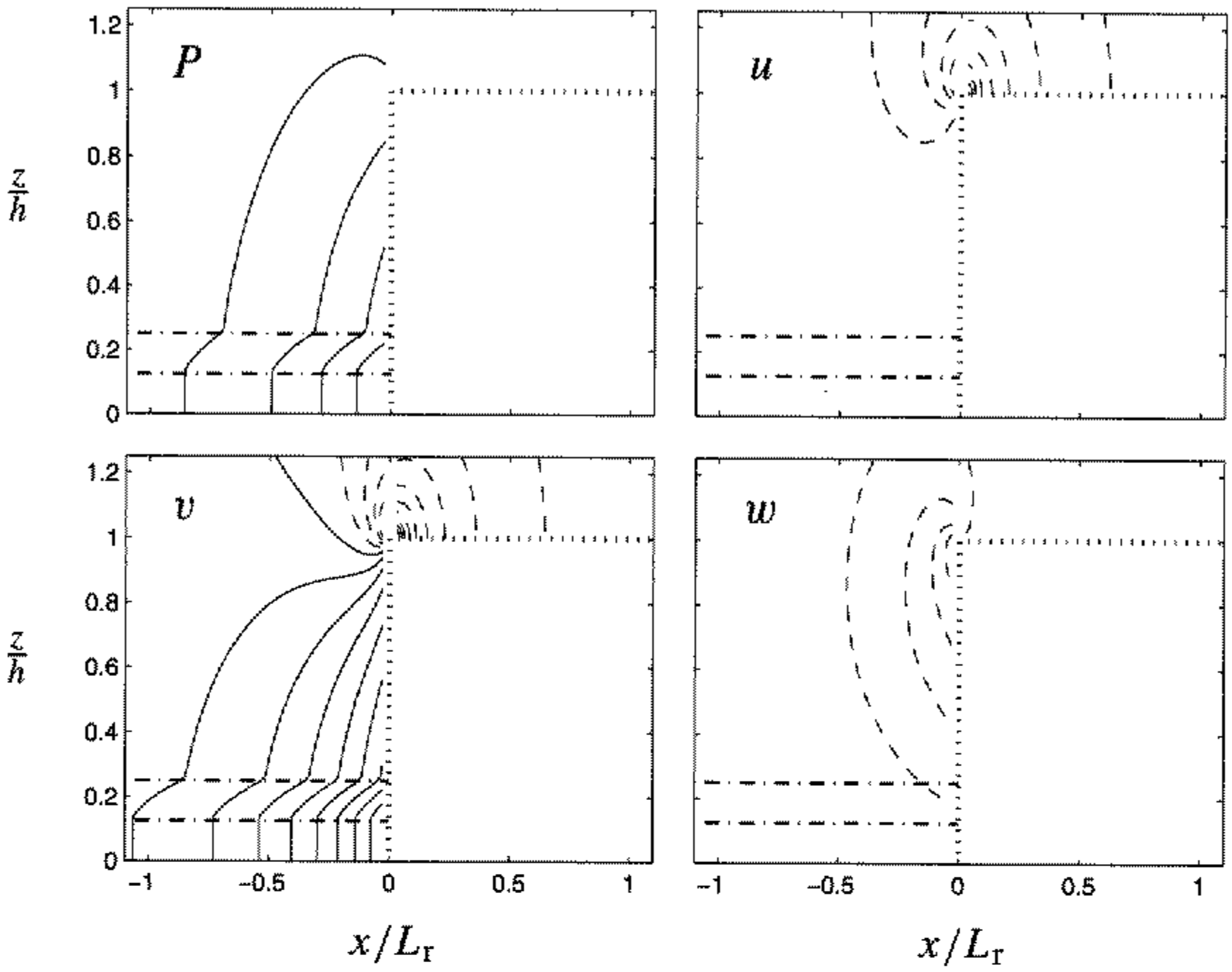

Figure 8. As in Fig. 7, except that $h = 2$ km and only the lowest 30% of the domain is plotted. The contour interval for u and v is 0.0058 m s^{-1}, and for w it is 7.1×10^{-5} m s^{-1}.

mode-0 step-trapped Kelvin wave appear as shown in Fig. 7. This mode is again obtained by setting $\lambda = 1$. The phase speed for this mode is 4.9 m s^{-1}, $\lambda_y = 389$ km, and $\omega/f = 0.79$. The perturbations in v and P are strongest in the layer below the inversion, which might lead one to suppose that the disturbance is vertically trapped by the inversion. The perturbations in u and w are, however, very similar to those for the mode-0 wave in an atmosphere with uniform Brunt–Väisälä frequency (cf. Fig. 4) and, in reality, the wave shown in Fig. 7 is vertically trapped because it is sub-inertial and the height of the vertical step is finite.

The inability of the inversion to prevent vertical energy propagation in step-trapped Kelvin waves is more apparent if one considers the case shown in Fig. 8 in which h is increased to 2 km, but all other physical parameters are held fixed. In this case the perturbations in v and P extend well above the MBL, and it is clear that the actual limitation on their vertical extent is associated with the finite height of the topography. The phase speed of this mode is 10.0 m s^{-1}, $\lambda_y = 902$ km, and $\omega/f = 0.70$.

Of course one would not use a shallow-water model to study the vertical structure of disturbances in an internally stratified fluid, but one might hope that the reduced-gravity shallow-water model is at least capable of predicting the phase speed of these waves when there is a pronounced inversion capping the MBL. Using the 250 m height of the base of the inversion layer* to define the undisturbed depth of the shallow-water layer D, the linearized reduced-gravity shallow-water equations support Kelvin waves moving at a phase speed of 8.75 m s^{-1} . Shallow-water Kelvin waves are non-dispersive,

* The difference between the phase speeds of shallow-water Kelvin waves and step-trapped Kelvin waves is not systematically reduced by using the middle or the top of the marine inversion to define the top of the shallow-water layer.

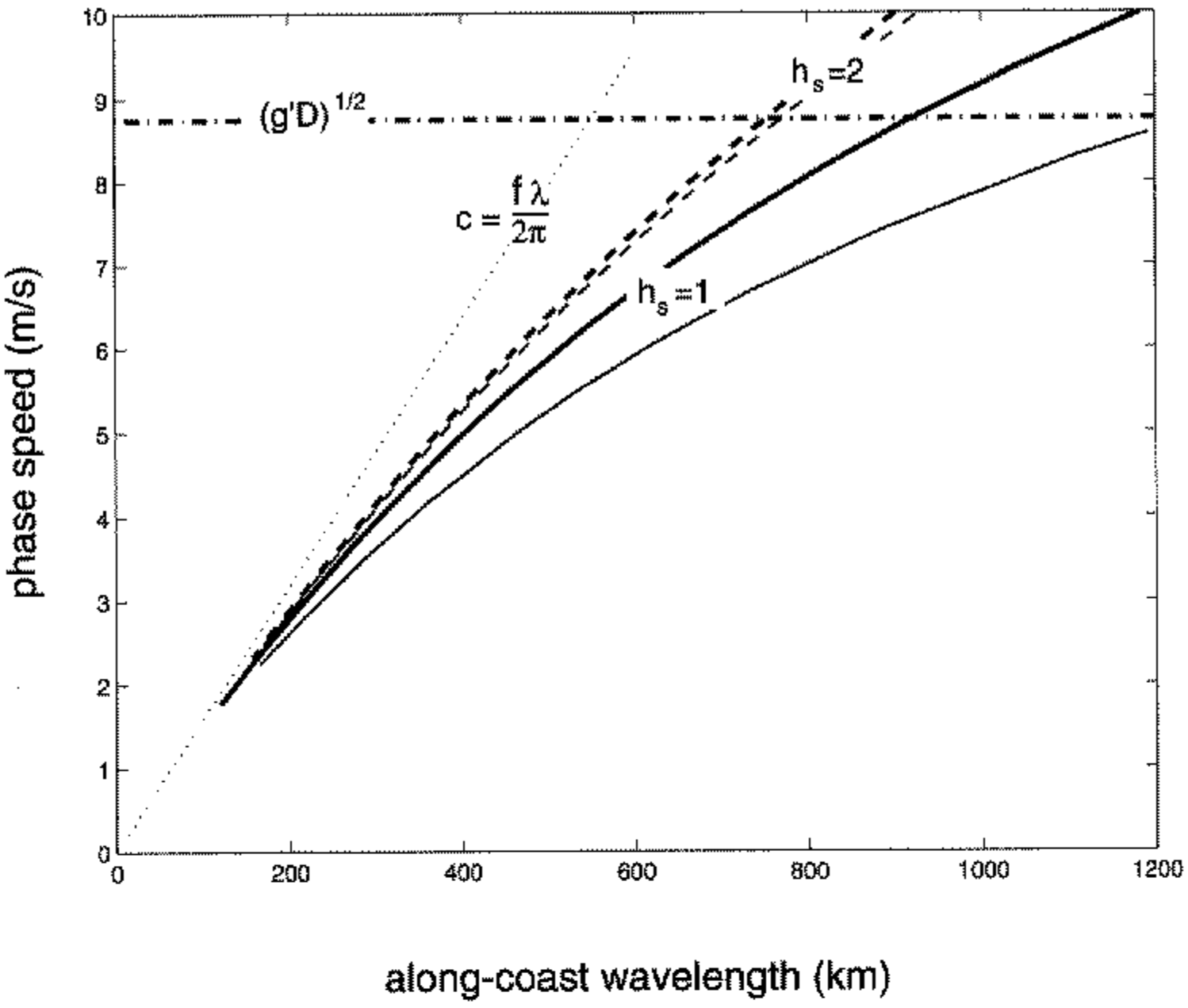

Figure 9. Phase speed as a function of along-step wavelength for the reduced-gravity shallow-water model (dot-dashed line) and for mode-0 step-trapped Kelvin waves when the topographic barrier is 1 km high (solid lines) or 2 km high (dashed lines). Data for the case with an idealized MBL and capping inversion are shown by the thick lines; the thin lines are for the case with uniform stability. Also shown as a reference is the line $c = f\lambda_y/(2\pi)$ (thin dotted line).

but the internal waves that are actually supported by this system (the step-trapped Kelvin waves shown in Figs. 7 and 8) are dispersive. The phase speeds for shallow-water Kelvin waves and for mode-0 step-trapped Kelvin waves are plotted as a function of the along-step wavelength in Fig. 9. As is apparent in Fig. 9, the reduced-gravity shallow-water model does not provide a reliable estimate of the true phase speed of step-trapped Kelvin waves, which are a strong function of λ_y and a somewhat weaker function of the mountain height. All step-trapped Kelvin waves are sub-inertial and the phase-speed curves for these waves asymptote to the line $c = f\lambda_y/(2\pi)$ as $\lambda_y \to 0$ which, of course, is completely different from the reduced-gravity shallow-water result that $c = \sqrt{g'D}$.*

The influence of atmospheric structure on the phase speed of step-trapped Kelvin waves can be seen by comparing the speeds of the eigenmodes when an MBL and strong capping inversion is present (heavy dashed and solid lines) with those eigenmodes for an atmosphere with uniform Brunt–Väisälä frequency (thin dashed and solid lines). In the case of the two-kilometre-high barrier, the mode-0 eigenmode is almost completely insensitive to the presence of the idealized MBL and capping inversion. When the step is 1 km high, however, the mode-0 step-trapped Kelvin wave is much more sensitive to the presence of the MBL.

Perhaps the most interesting influence of the idealized MBL and capping inversion on the structure of Kelvin waves trapped against a one-kilometre-high step occurs in the mode-2 wave, for which the perturbation pressure and velocity fields in an x–z cross section are shown in Fig. 10. As before, this mode was computed for the case

* Although the hydrostatic approximation, used in both the shallow-water model and in (11), becomes invalid in the limit $\lambda_y \to 0$, the difference between the phase speeds of shallow-water Kelvin waves and step-trapped Kelvin waves becomes significant at values of λ_y for which the hydrostatic approximation remains appropriate.

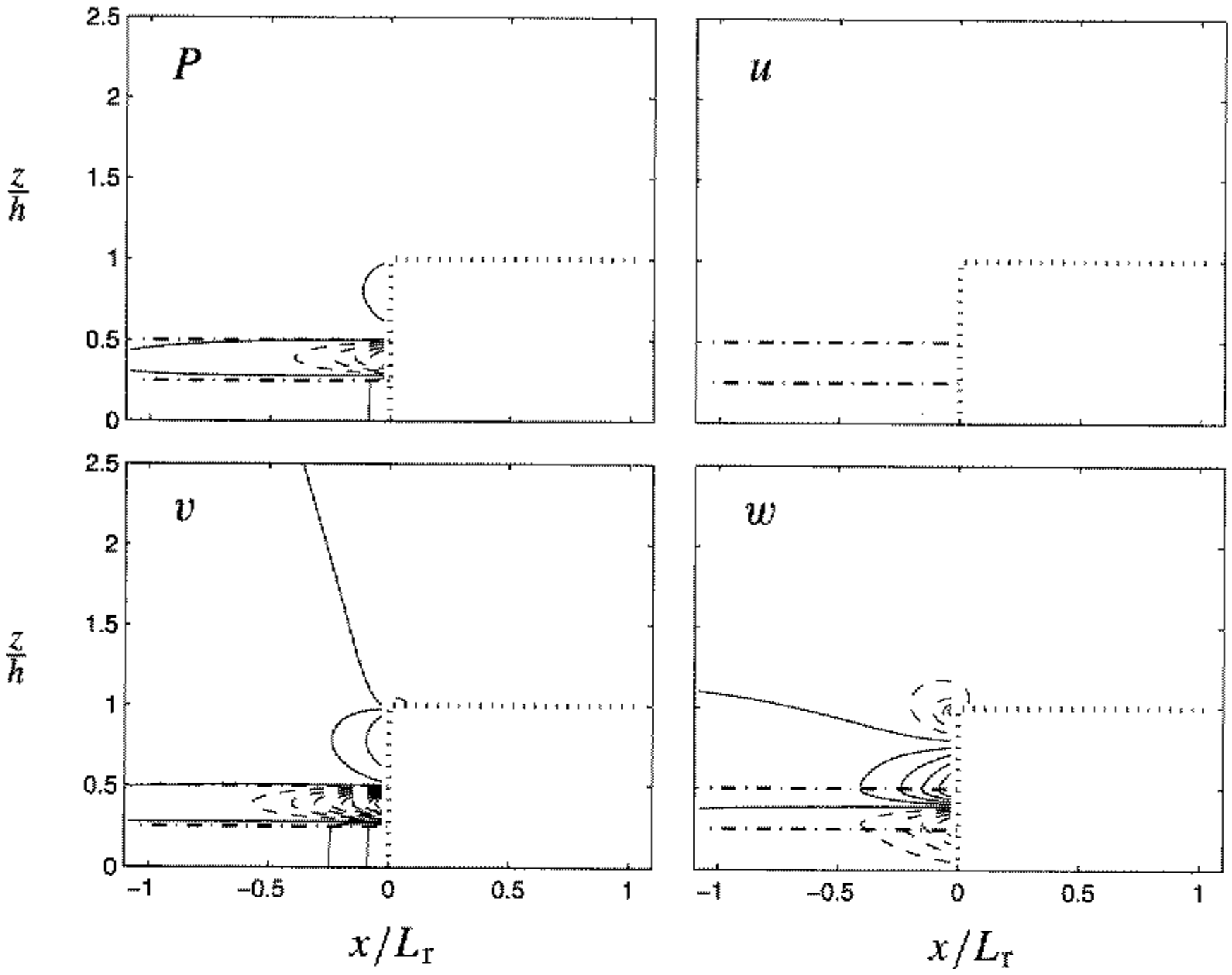

Figure 10. Cross-sections showing the x–z structure of the mode-2 wave in the presence of an idealized MBL and capping inversion. As in Fig. 7, except that the contour interval for P is 0.8, for u and v it is 0.16 m s^{-1}, and for w it is 2.2×10^{-4} m s^{-1}.

$\lambda = 1$; its phase speed is 2.13 m s^{-1}, $\lambda_y = 610$ km, and $\omega/f = 0.24$. The strongest perturbations in this mode are concentrated in the inversion layer in a manner similar to that observed during the 10–11 June 1994 CTD off the central California coast (Ralph *et al.* 1998, Fig. 23). Since the MBL and capping inversion specified in this idealized problem are derived from the thermodynamic profile upstream of the 10–11 June 1994 CTD, the similarity in the observed and computed vertical structures suggests the simplified mathematical model presented in this paper is not idealized beyond all practical application. Nevertheless, it should be noted that the 2 m s^{-1} phase speed of the mode-2 wave is more than a factor of four slower than that of the actual CTD. On the other hand, the 7–8 m s^{-1} phase speed of a typical CTD is close to that of a mode-0 step-trapped Kelvin wave with a physically reasonable along-barrier wavelength of $\lambda_y = 700$ km (see Fig. 9). A more detailed comparison between theory and observation cannot be conducted without a more accurate representation of the topography, the inclusion of low-level northerly flow in the reference-state profile and some assessment of the importance of nonlinear processes. It is difficult to include a vertically sheared mean flow in the preceding semi-analytic model, so more realistic basic-state flows will not be considered in this paper. The influence of more realistic topography and nonlinear processes will discussed in the next section.

5. Finite slopes and nonlinearity

It is not possible to use the preceding methodology to compute the eigenmodes supported by a more realistic topographic profile in which the vertical step in the topography is replaced by a slope of finite width. At least in principle, the structure of

such modes could be determined by fully numerical techniques like resonance iteration (Wang and Mooers 1976) and inverse iteration (Huthnance 1978). These numerical methods, and refinements thereof, have been used to compute coastal-trapped waves in both idealized and realistic ocean basins. In most oceanic applications the surface of the ocean provides a natural upper boundary that limits the depth of the fluid through which computations need to be performed, and thereby limits the size of the numerical domain and the total computer time required to obtain an accurate solution.* Even in the relatively recent work by Webster and Holland (1987), the numerical solution is obtained on a comparatively coarse 25×17 vertically stretched grid. Recall that, in order to remove any sensitivity to the upper boundary and to adequately resolve the structure of the MBL and capping inversion, the calculations in this paper were performed with at least 241 grid points along the vertical coordinate. A very considerable computational effort is thus required to obtain the equivalent of Fig. 7 for topography with a finite slope, and such computations were not attempted in this study. Some gain in efficiency might be realized using the solution procedure of Schmidt and Johnson (1993a), however their approach is not immediately applicable to the physically important, lowest-order mode for which ω/f is O(1).

Considerably fewer grid points are required if one does not have to resolve the marine inversion in the basic-state flow accurately. In particular, much less computational effort is required to evaluate the trapped modes supported by a smooth ridge in a fluid in which the basic-state Brunt–Väisälä frequency is constant. Calculations of this type have been performed by Brink (1989) in an investigation of seamount-trapped waves. Brink computed the structure of the eigenmodes that freely orbit an idealized seamount and, in agreement with the behaviour of the step-trapped Kelvin waves presented in this paper, he found that those modes that were bottom trapped were sub-inertial. The finding that bottom-trapped waves are sub-inertial is also consistent with the analysis of Rhines (1970), who obtained solutions for boundary-trapped eigenmodes in a continuously stratified fluid bounded by an infinite plane tilted off the horizontal at an arbitrary angle. Further evidence that the vertical trapping of more general types of CTD is not dependent on the presence of an elevated inversion is provided by the recent nonlinear numerical simulations by Skamarock *et al.* (1999). They found that CTD-like disturbances could be created in response to a localized off-shore flow both in an atmosphere with a typical marine layer and capping inversion and in an atmosphere with uniform Brunt–Väisälä frequency.

Skamarock *et al.* (1999) emphasized the importance of nonlinearity in creating a realistic CTD-like response. Shallow-water theory provides some of the simplest mathematical descriptions of nonlinear fluid-dynamical processes, and it is likely that nonlinear CTD are qualitatively analogous to nonlinear shallow-water Kelvin waves. The qualitative similarity, and quantitative differences, between nonlinear shallow-water flow over an obstacle and downslope windstorms in the atmosphere have already been established in several previous studies (Smith 1985; Durran 1986; Durran and Klemp 1987; Bacmeister and Pierrehumbert 1988; Durran 1992), all of which suggest that strong downslope winds can be produced when the atmosphere undergoes a transition analogous to that from subcritical to supercritical flow in the shallow-water model. Nevertheless, Durran (1986) did demonstrate that these atmospheric analogues to subcritical and supercritical flow cannot be distinguished by the sign of $F' - 1$, where F' is the Froude

* The surface of the ocean also serves as physical boundary that clearly limits upward energy propagation by coastal-trapped waves. As a consequence, the question of vertical energy propagation examined in this paper does not seem to have been addressed in papers on oceanic coastal-trapped waves.

number for the reduced-gravity shallow-water model,

$$F' = \frac{U}{\sqrt{g'D}}, \tag{28}$$

U is average the speed of the flow in the layer between the ground and the base of the elevated inversion, and D is the depth of that layer.

As in the case of downslope windstorms, the most useful connection between the dynamics of inversion-capped MBL and shallow-water theory may be primarily qualitative. In particular, the results presented in this paper suggest that there is no theoretical basis for quantitatively distinguishing between supercritical and subcritical flows within the marine boundary layer by computing a local Froude number (F') based on the depth of the marine layer and the temperature change across the inversion. In classical shallow-water theory the Froude number represents the ratio of the flow speed to the shallow-water gravity-wave speed. However, as shown in Fig. 9, those linear waves that are actually supported by a strong elevated inversion seaward of a step mountain may move at speeds quite different from the phase speed for Kelvin waves predicted by the reduced-gravity shallow-water model. Thus, the conventional shallow-water Froude number does not have the same physical interpretation as the Froude number for the reduced-gravity shallow-water model, because, F' is generally not the ratio of the flow speed to the phase speed of any particularly significant linear wave.

6. Conclusions

It has been shown that an infinitely deep, stably stratified fluid can support vertically-trapped *hydrostatic* modes that propagate parallel to the face of an uninterrupted topographic step. These modes have been referred to as *step-trapped Kelvin waves*, because their structure in the region below the top of the step is very similar to that of a classical internal Kelvin wave in a stratified fluid bounded by a free surface at the same height as the top of the step. Step-trapped Kelvin waves are laterally trapped by the Coriolis force and vertically trapped because their frequencies are less than f and, at least to within the accuracy of the f-plane approximation, no sub-inertial disturbance can propagate vertically through the laterally unbounded atmosphere above the topographic step. It should be emphasized that none of these hydrostatic modes would be vertically trapped if the the topographic step was infinitely high, because there is no low-frequency limit on the vertical propagation of classical internal Kelvin waves.

Step-trapped Kelvin-wave solutions were obtained for two basic states: one with uniform stratification throughout the fluid and one with an idealized MBL capped by a strong inversion. Although the marine inversion plays no fundamental role in preventing upward energy propagation in linear CTDs, the vertical structure of step-trapped Kelvin waves is significantly modified when a strong inversion caps the MBL. In particular, when the basic state is specified using an MBL and capping inversion characteristic of that during the 10–11 June 1994 central California CTD, the vertical structure of the mode-2 step-trapped Kelvin wave (see Fig. 10) is surprisingly similar to that actually observed during this event.

Many previous investigators have used the shallow-water equations to mathematically model hydrostatic motions within an MBL capped by a strong inversion. In these studies the linkage between the atmosphere and the shallow-water equations is not generally made by evaluating the normal modes for the full stratified equations, but rather by replacing the gravitational acceleration in the standard single-layer shallow-water model with a reduced gravity proportional to g times the potential-temperature (or density)

difference across the capping inversion, and by replacing the fluid depth in the standard model with the depth of the MBL. This 'reduced-gravity shallow-water model' is clearly an approximation because it assumes that all pressure perturbations within the MBL are produced by vertical displacements of the capping inversion. The results presented in this paper suggest that at least some aspects of this approximation are not very good.

The phase speeds of Kelvin-wave solutions to the linearized reduced-gravity shallow-water equations were compared with those of the hydrostatic linear step-trapped Kelvin waves supported by a basic state with an idealized MBL and a strong capping inversion. The phase speeds predicted by these two approaches were generally in poor agreement, not only with respect to the numerical values, but also in the sense that step-trapped Kelvin waves are dispersive whereas shallow-water Kelvin waves are non-dispersive. (see Fig. 9). Thus, the reduced-gravity shallow-water model does not appear to provide an accurate description of the linear dynamics of CTDs.

Nevertheless, the preceding is not meant to suggest that shallow-water theory is completely irrelevant to the dynamics of CTDs or inversion-capped marine layers. As is the case with downslope windstorms, considerable evidence has been compiled demonstrating a qualitative similarity between the nonlinear behaviours of the shallow-water and continuously stratified systems. In particular, both systems appear to undergo a transition from a state where disturbance energy can be efficiently radiated away by wave propagation (subcritical flow) to a state in which energy transport is largely accomplished by horizontal advection (supercritical flow). Nevertheless, caution is advised when attempting to characterize marine-layer flows as supercritical or subcritical using a Froude number defined on the basis of the reduced-gravity shallow-water model in a manner similar to (28). One source of concern is simply the uncertainty in the computation of F'. In many real-world applications there is sufficient vertical variation in the wind profile, lack of definition at the top of the inversion, and uncertainty in the depth of the MBL that it is rather difficult to unambiguously determine a numerical value for F'. Even more fundamental, however, is the difficulty of determining the precise physical significance of F' because, in contrast to the conventional shallow-water Froude number, F' need not represent the ratio of a flow speed to the speed of any particularly significant linear wave.

ACKNOWLEDGEMENTS

The author has greatly benefited from helpful discussions with Rajul Pandya, Rich Rotunno and Roger Samelson. This research was sponsored by an Office of Naval Research grant N00014-93-1-1304 and National Science Foundation grants ATM-9530662 and ATM-9817728.

REFERENCES

Bacmeister, J. T. and Pierrehumbert, R. T. 1988 On high-drag states of nonlinear stratified flow over an obstacle. *J. Atmos. Sci.*, **45,** 63–80

Bannon, P. R. 1981 Synoptic-scale forcing of coastal lows; forced double Kelvin waves in the atmosphere. *Q. J. R. Meteorol. Soc.*, **107,** 313–327

Bond, N. A., Mass, C. F. and Overland, J. E. 1996 Coastally trapped wind reversals along the United States west coast during the warm season. Part I: Climatology and temporal evolution. *Mon. Weather Rev.*, **124,** 430–445

Brink, K. H. 1989 The effect of stratification on seamount-trapped waves. *Deep-Sea Res.*, **36,** 825–844

Chapman, D. C. 1982 On the failure of Laplace's tidal equations to model subinertial motions at a discontinuity in depth. *Dyn. Atmos. Ocean.*, **7,** 1–16

Dorman, C. 1985 Evidence of Kelvin waves in California's marine layer and related eddy generation. *Mon. Weather Rev.*, **113,** 827–839

Durran, D. R. 1986 Another look at downslope windstorms. Part I: The development of analogs to supercritical flow in an infinitely deep, continuously stratified fluid. *J. Atmos. Sci.*, **43,** 2527–2543

1992 Two-layer solutions to Long's equation for vertically propagating mountain waves: How good is linear theory? *Q. J. R. Meteorol. Soc.*, **118,** 415–433

Durran, D. R. and Klemp, J. B. 1987 Another look at downslope windstorms. Part II: Nonlinear amplification beneath wave-overturning layers. *J. Atmos. Sci.*, **44,** 3402–33412

Freeman Jr., J. C. 1948 An analogy between equatorial easterlies and supersonic gas dynamics. *J. Meteorol.*, **5,** 138–146

Gill, A. E. 1977 Coastally trapped waves in the atmosphere. *Q. J. R. Meteorol. Soc.*, **103,** 431–440

1982 *Atmosphere–ocean dynamics*. Academic Press

Holland, G. J. and Leslie, L. M. 1986 Ducted coastal ridging over S.E. Australia. *Q. J. R. Meteorol. Soc.*, **112,** 731–748

Huthnance, J. M. 1978 On coastal-trapped waves: Analysis and numerical calculation by inverse iteration. *J. Phys. Ocean.*, **8,** 74–92

Long, R. R. 1954 Some aspects of the flow of stratified fluids II. Experiments with a two-fluid system. *Tellus*, **6,** 97–115

Nance, L. B. and Durran, D. R. 1997 A modeling study of nonstationary trapped mountain lee waves. Part I: Mean flow variability. *J. Atmos. Sci.*, **54,** 2275–2291

Nguyen Ngoc Anh and Gill, A. 1981 Generation of coastal lows by synoptic-scale waves. *Q. J. R. Meteorol. Soc.*, **107,** 521–530

Ralph, F. M., Armi, L., Bane, J. M., Dorman, C., Neff, W. D., Neiman, P. J., Nuss, W. and Persson, P. O. G. 1998 Observations and analysis of the 10–11 June 1994 coastally trapped disturbance. *Mon. Weather Rev.*, **126,** 2435–2465

Reason, C. J. C. and Steyn, D. G. 1992 The dynamics of coastally trapped mesoscale ridges in the lower atmosphere. *J. Atmos. Sci.*, **49,** 1677–1692

Rhines, P. 1970 Edge-, bottom-, and Rossby waves in a rotating stratified fluid. *Geophys. Fluid Dyn.*, **1,** 273–302

Rogerson, A. M. and Samelson, R. M. 1995 Synoptic forcing of coastal-trapped disturbances in the marine atmospheric boundary layer. *J. Atmos. Sci.*, **52,** 2025–2040

Samelson, R. M. 1999 The vertical structure of linear coastal-trapped modes. *Mon. Weather Rev.*, **127,** 201–213

Samelson, R. M. and Rogerson, A. M. 1996 Life cycle of a linear coastal-trapped disturbance. *Mon. Weather Rev.*, **124,** 1853–1863

Schmidt, G. and Johnson, E. 1993a Direct calculation of low-frequency coastally trapped waves and their scattering. *J. Atmos. Ocean. Technol.*, **10,** 368–380

1993b Grid dependence in the numerical determination of topographic waves. *Ocean Modelling*, **98,** 10–11

Scorer, R. 1949 Theory of waves in the lee of mountains. *Q. J. R. Meteorol. Soc.*, **75,** 41–56

Skamarock, W. C., Rotunno, R. and Klemp J. B. 1999 Models of coastally trapped disturbances. *J. Atmos. Sci.*, **56,** 3349–3365

Smith, R. B. 1985 On severe downslope winds. *J. Atmos. Sci.*, **42,** 2597–2603

Wang, D.-P. and Mooers, C. N. K. 1976 Coastal-trapped waves in a continuously stratified ocean. *J. Phys. Ocean.*, **6,** 853–863

Webster, I. and Holland, D. 1987 A numerical method for solving the forced baroclinic coastal-trapped wave problem of general form. *J. Atmos. Ocean. Technol.*, **4,** 220–226

Winant, C. D., Dorman, C. E., Friehe, C. A. and Beardsley, R. C. 1988 The marine layer off northern California: An example of supercritical channel flow. *J. Atmos. Sci.*, **45,** 3588–3605